CORE
Metadata, citation and similar papers at core.ac.uk
Provided by epublications@Marquette

Marquette University
e-Publications@Marquette

Electrical and Computer Engineering Faculty Research and Publications
Electrical and Computer Engineering, Department of

6-1-2015

Investigation of the Surface Adhesion Phenomena and Mechanism of Gold-Plated Contacts at Superlow Making/Breaking Speed

Wanbin Ren
Harbin Institute of Technology

Cheng Chang
Harbin Institute of Technology

Yu Chen
Harbin Institute of Technology

Shengjun Xue
Harbin Institute of Technology

Ronald A. Coutu Jr.
Marquette University, ronald.coutu@marquette.edu

Accepted version. *IEEE Transactions on Components, Packaging and Manufacturing Technology*, Vol. 5, No. 6 (June 2015): 771-778. DOI. © 2018 IEEE. Used with permission.
Ronald A. Coutu, Jr. was affiliated with the Department of Electrical and Computer Engineering, Air Force Institute of Technology, Wright-Patterson AFB, OH at the time of publication.

Marquette University

e-Publications@Marquette

Electrical and Computer Engineering Faculty Research and Publications/College of Engineering

***This paper is NOT THE PUBLISHED VERSION;* but the author's final, peer-reviewed manuscript.**
The published version may be accessed by following the link in the citation below.

IEEE Transactions on Components, Packaging and Manufacturing Technology, Vol. 5, No. 6, (June, 2015): 771-778. DOI. This article is © Institute of Electrical and Electronic Engineers (IEEE) and permission has been granted for this version to appear in e-Publications@Marquette. IEEE does not grant permission for this article to be further copied/distributed or hosted elsewhere without the express permission from IEEE.

Contents

Abstract: ... 2
SECTION I. Introduction ... 2
SECTION II. Experimental Setup and Measurements ... 3
SECTION III. Discussion ... 7
A. Physical Mechanism of Adhesion Force ... 9
B. Relationship Between Adhesion Resistance and Adhesion Force ... 12
SECTION IV. Conclusion ... 16
References ... 16

Investigation of the Surface Adhesion Phenomena and Mechanism of Gold-Plated Contacts at Superlow Making/Breaking Speed

Wanbin Ren

School of Electrical Engineering and Automation, Harbin Institute of Technology, Harbin, China

Cheng Chang

School of Electrical Engineering and Automation, Harbin Institute of Technology, Harbin, China

Yu Chen

School of Electrical Engineering and Automation, Harbin Institute of Technology, Harbin, China

Shengjun Xue

School of Electrical Engineering and Automation, Harbin Institute of Technology, Harbin, China

Ronald A. Coutu

Department of Electrical Computer Engineering, Air Force Institute of Technology, Wright-Patterson AFB, OH

Abstract:

Surface adhesion phenomena of gold-plated copper contact materials are studied in conditions of nonarc load (5/15/25 V and 0.2/0.5/1 A) and superlow speed (25 and 50 nm/s) realized by a piezoactuator during the making and breaking processes. It is shown that softening and melting of local asperities leads to interface adhesion, which results from the joule heat generated by the contact resistance; it is determined that the change of contact force with time obeys the negative exponential distribution and the time constant is associated with the adhesion force directly. Based on the fitting experimental data, the relationship between the adhesion force F_z and the contact resistance R_d while breaking can be expressed as $F_z \propto {R_d}^{-1}$, which indicates that the main component of contact resistance is the bulk resistance of weld nugget and the constriction resistance is negligible.

SECTION I. Introduction

Nowadays, surface metal coatings are becoming increasingly important in modern electronic and electrical industries. Such trends are driven by many useful functions offered by the coatings such as corrosion and wear protection, diffusion barriers, conductive circuit elements, fabrication of passive devices on dielectric surfaces, and others.[1] Remarkably, gold-plated contacts, which offer the advantages of low and stable electrical contact resistance and thermal contact resistance, and high off isolation, are widely used in miniature electromagnetic relays,[2] electrical connectors,[3] integrated circuits,[4] thin-film devices,[5] and microelectromechanical system (MEMS).[6–7,8] Despite these unique attributes, typical failure phenomena including surface adhesion (also called stiction), contact welding, and intermittency still occur during electrical contact events and remain a concern.[9,10,11,12,13] To our knowledge, the dominant physical failure mechanisms of surface adhesion for gold-plated electrical contact material are not fully understood yet. Therefore, the current situation offers both challenges and opportunities for miniaturization of traditional electromechanical devices and practical MEMS switches.

In general, the electrical contact behavior is defined as the relationship between the contact voltage or contact resistance versus the contact force during loading and unloading events. Moreover, such behaviors are complicated by a thermal–electrical–mechanical coupled field, partial asperity melting,

and phase transitions that coexist at the interface.[14,15] It has been proved that adhesion phenomenon between contact materials is directly related to the physical properties of the contact metal materials (hardness, electrical conductivity, thermal conductivity, etc.), surface condition (surface roughness and surface film's properties), mechanical parameters (making/breaking speed and contact force), environmental atmosphere parameters (temperature, humidity, and atmosphere), and electrical parameters (carrying current, open voltage).[1]

It is reported that the maximum breaking velocity of an electromagnetic relay is perhaps the magnitude of several hundred millimeters per second.[16] The adhesion phenomenon is mainly attributed to the transient melting of contact surface under this velocity. These random characteristics of adhesion force (or welding force) offer both measurement challenges and difficulties for determining the adhesion physical mechanism. The joule heat duration is correspondingly extended when contact velocity is reduced. Thus, it would be beneficial for us to know the root cause and influencing factors about the adhesion. If we take the order of micrometers per second as a low velocity, then the order of nanometers per second used is considered as a superlow velocity in this paper.

The studies of properties and mechanism of material surface adhesion are always hot topics in the field of metal interface physics. Kwon *et al.*[17] investigated the relationship between contact resistance and contact force during making and breaking operations of glass substrate with gold coating and found that the adhesion phenomenon was the result of van der Waals force or the binding force between metallic bonds. Tringe *et al.*[18] stated that the contact resistance and adhesive properties of Au/Au contact interface were determined by the adsorption film of pollution using an interfacial force microscopy. Patton and Zabinski[19] proposed that electrical current had a profound effect on surface adhesion of Au coatings and concluded that adhesion was linked to the creation of a smooth surface texture and associated van der Waals forces. They also observed that aging of the contacts in air could reduce adhesion. Gregori and Clarke[20] evaluated the adhesion characteristics with repeated actuation and proposed that the increase in adhesive force was attributed to mechanical creep of the gold contacts. The velocity reported in[17] is 30 nm/s and that used in[18] is 4.2 nm/s. In addition, Miyanaga *et al.*[21–22,23,24] researched on the generation and break of the molten bridge at a low speed of 100–300 μm/s and found that the length and diameter of molten bridge are affected by the heat conditions, including the thermal conductivity and the velocity of the heat flow.

In this paper, we devised an *in situ* contact measurement apparatus to examine the effect of the current load condition on electrical contact behaviors of Au-plated contacts. From this, the physical mechanism of occurred adhesion during contact breaking is discussed under different load voltages and load currents. Next, the adhesion resistance was defined and the relationship between adhesion resistance and adhesion force is examined. Finally, we proved that the intrinsic characteristics of adhesion resistance is bulk resistance of the welded nugget; its knowledge is essential to understand the formation and rupture process of adhesion at superlow making and breaking speeds.

SECTION II. Experimental Setup and Measurements

The *in situ* contact measurement apparatus consists of four main modules including a 4-DOF motion structure, a measurement unit, software control, and an auxiliary optical camera that are shown in Fig. 1. The horizontal actuation of the moving electrode was obtained by means of a precision slider that was pushed by a piezoelectric actuator (LTC2013-013, PiezoMotor AB, Sweden). The motion velocity can

be set between 5 nm/s and 12 mm/s. The desired displacement of the moving electrode was controlled by the motor driver with a position feedback loop, which was provided by the assembled grating ruler (RGH25F-5 nm, Renishaw, U.K.). Fig. 2 shows the schematic of the experimental circuit. The motor driver (PMD101, PiezoMotor AB, Sweden) received the controlling instruction from the personal computer (PC) and provides closed-loop control for Piezomotor by reading the feedback position of grating ruler, which had a displacement resolution of 5 nm and at a 10-Hz sampling rate.

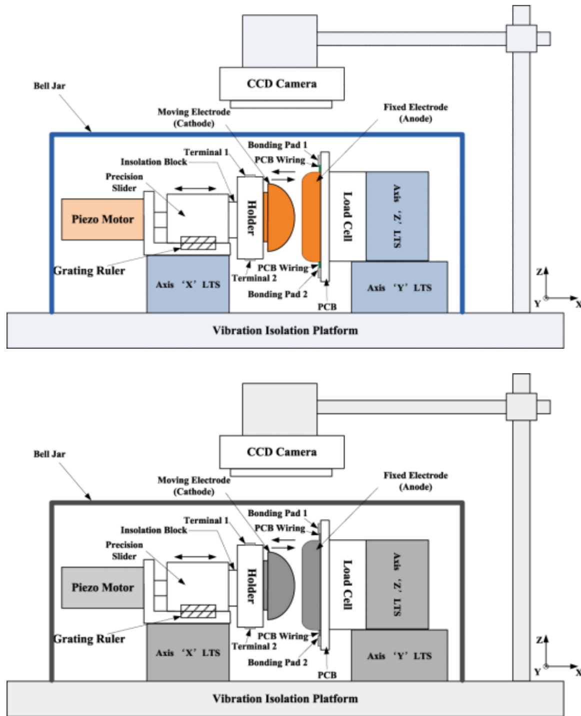

Fig. 1. Schematic of the test rig.

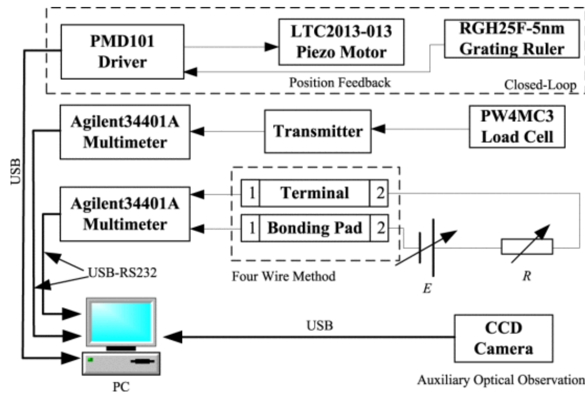

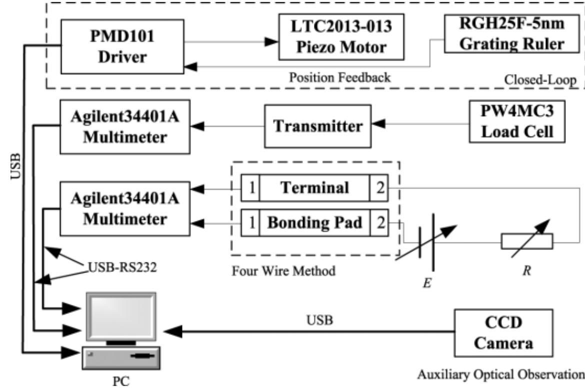

Fig. 2. Experimental circuit.

The shank of the fixed contact was welded on the printed circuit board (PCB) to clamp the electrode and its two terminals can be extended to the lateral bonding pads through PCB wirings. Using the four-wires method, the instantaneous value of contact voltage drop was continuously measured besides the corresponding contact force. The normal contact force between two electrodes was assessed using a strain sensor (PW_4MC_3, HBM, Germany), which had the measurement range of 3 N and a resolution of 5 mN. Additional one and two combined linear translation stages were connected with the moving part and fixed part, respectively, for manual adjustment. The whole mechanical part was placed in a dust-tight transparent Plexiglas housing that was secured on a bench-top isolation system (PWA090, Thorlabs, U.K.). The spatial relationship between two electrodes during experiment can be observed by the charge-coupled device camera (SJM-200C, China). During testing, the measured data were simultaneously acquired by two multimeters (34401A, Agilent, USA) followed by uploading to the PC. The multimeters had the resolutions of 1 μV and the integration time of 10NPLC. The microstepping number of 10 steps per second and the step length of 5 nm are configured for the piezoactuator, so the average making and breaking velocity is 50 nm/s. Therefore, the sampling rate of 2.5 Hz fully meets the sampling requirement of piezoacturator in superslow motion. The moving electrode is a hemisphere-shaped rider, with a diameter of 2 mm, and the fixed electrode is a flat sample, both made of copper alloy and electroplated with Au (1-μm thick). The roughness was measured using a confocal optical microscope (LEXT 3000, Olympus) and resulting in a surface roughness below 0.8 μm. To remove the film in the samples surface, we kept them under the condition of high temperature 120 °C and relative humidity 80% for more than 24 h, and then degreased using acetone, alcohol, and distilled water in an ultrasonic cleaner, and dried and carefully mounted in the test measurement apparatus. The details of the experimental conditions used are detailed in Table I.

TABLE I Details of the Experimental Conditions Used in This Paper

Parameter	Value
Expected contact force F_c	50mN
Making & Breaking Velocity v	25,50nm/s
Load Voltage U	5,15,25 V
Load Current I	0.2,0.5,1 A
Environment	Temperature 19℃-22℃ Humidity 57% RH

Prior to the experiment, the source voltage is set as the open-circuit voltage (also called load voltage U) and the load current I is set by the adjustable resistor in the contact-closed position. The loading and unloading motor speeds are both set as v, while the expected contact force is designated as F_C. Scanning electron microscopy (Helios Nanolab 600i, FEI, USA) was used to characterize the adhesion area.

Fig. 3 shows a comparison example of the measured variation of the contact force and contact voltage of gold-to-gold contacts as a function of actuation time with and without current loading. The velocity of the actuator movement was maintained at 50 nm/s, as the piezoactuator pushes the contacts together. For the current loading case, the whole process is divided into the following stages.

1. *A (The Initial Contact):* Start of the electrical contact and an abrupt decline in contact voltage from 15 to 0.16 V occurred.
2. *A-B (The Softening and Melting Stage):* The contact force increased nonlinearly; meanwhile the contact voltage kept decreasing sharply.
3. *B-C (The Linear Loading Stage):* The contact force increases linearly to the expected value of 50 mN and the contact voltage stabilizes at 2 mV.
4. *C-D (The Linear Unloading Stage):* The contact force linearly decreases to zero with no significant change in the contact voltage.
5. *D-E (The Adhesive Stage):* The contact force shifts to an increasing tensile force and the corresponding contact voltage begins to increase. The largest value of tensile force is defined as the adhesion force F_Z.
6. *E-F (The Mechanical Breaking Stage/the Weld Breaking Stage):* The weld region of contacts breaks and the contact force restored to zero while the contact voltage jumps from 4 to 30 mV.
7. *F-G (The Metal Bridge Remelting Stage):* The contact force kept zero and the contact voltage fluctuates between 80 mV and 0.43 V with the feature of repeatedly rising up slowly and dropping down rapidly.
8. *G (The Electrical Breaking Stage):* The contact pairs were in electrical off status and the contact voltage returned to the load voltage U.

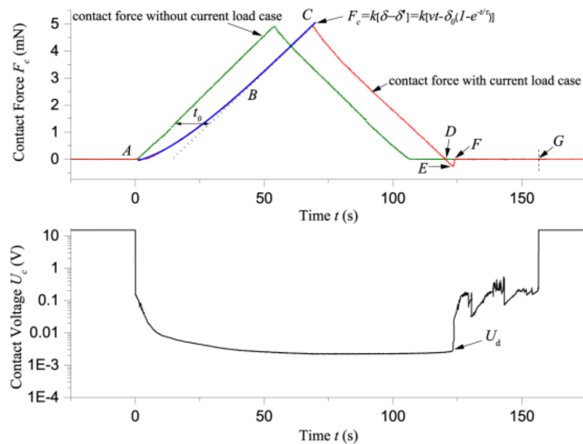

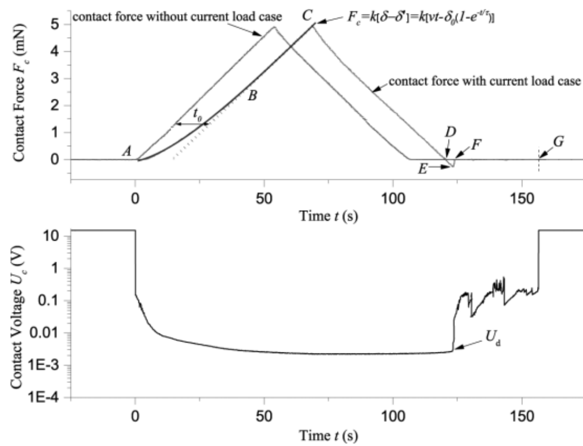

Fig. 3. Variation of contact force and contact voltage of Au-plated contacts as a function of the time during making and breaking (the speed is 50 nm/s and the load is 15 V/1 A).

As shown in Fig. 3, there are some apparent differences in A-B stage and D-E-F stage of the contact force curve in contrast to without current condition. It was clearly seen that the contact force curve presents a nonlinear softened spring trend in the loading stage and follows the linear trend, which is almost the same with the no current case. In addition, the slope of C-D segment and D-E segment, which belong to the contact force behavior curve, is consistent (shown in Fig. 3). This means that the two electrodes have bonded together completely. Therefore, the point E corresponds to the breaking moment of adhesion and the adhesion force F_z is 2.6 mN. The contact voltage at point E is defined as the breaking voltage U_d (4 mV in Fig. 3) and the contact resistance is defined as R_d. Since $U_d \ll U$, the current in D-E stage is considered to be constant and thus $R_d \approx U_d/I$. The contact resistance R_d increases with the piezoactuator position during the tension process in D-E phase and it is related to the adhesion force. The contact voltage in point E rises sharply, so U_d is easy to distinguish by this rising edge. R_d is defined as adhesion resistance, which means the contact resistance when adhesion occurs.

SECTION III. Discussion

Fig. 4(a) and (b) shows the variation of the contact force and contact voltage of Au-plated material as a function of the position of the piezoactuator, at two different electrical current loading conditions, respectively. In Fig. 4(a), the current is applied only when contact breaking. The whole process in Fig. 3 could be divided into the following stages: 1) A (force loading stage); 2) B (current loading initial point); and 3) C (unloading stage). For comparison, Fig. 4(b) shows the results of load current exerted only when contact making. The whole process in Fig. 4 could be divided into the following stages: 1) A (loading stage); 2) B (end of the current loading); and 3) C (force unloading stage). Combined with Fig. 3, the occurred contact adhesive phenomena are observed only when the current is applied in the contact making stage. In other words, the current applied in the contact making stage is the key factor of adhesion phenomenon. It appeared that from the data, the applied making current is the primary reason for the induced adhesion force.

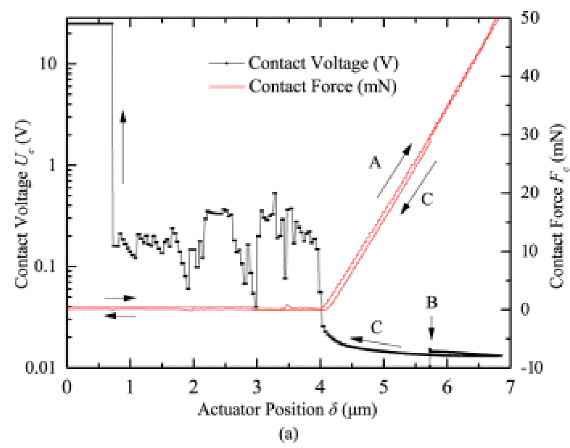

(a)

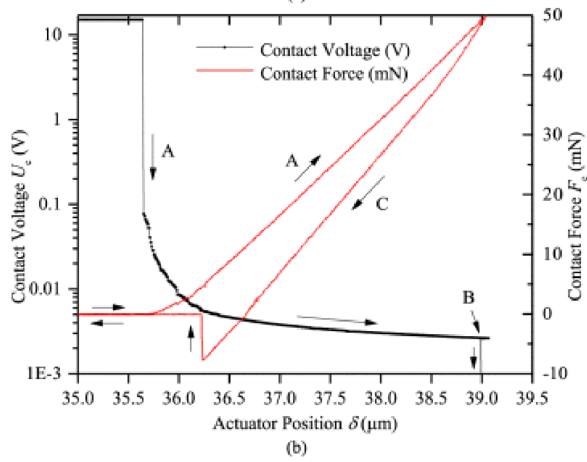

(b)

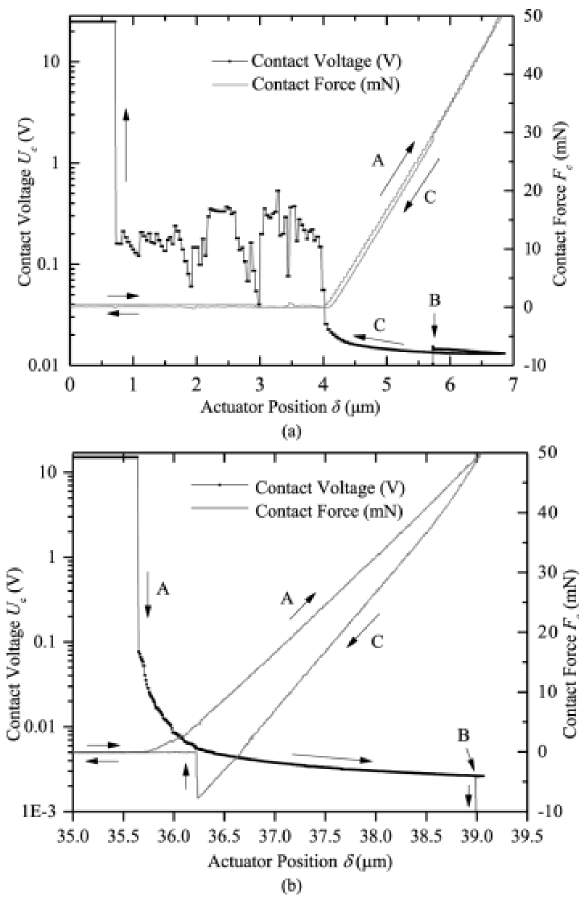

Fig. 4. Variation of contact voltage and contact force of Au-plated contacts as a function of the actuator position during making and breaking contacts (with a load voltage of 15 V, a load current of 1 A, and a speed of 50 nm/s). (a) Current is loading when contact breaking. (b) Current is loading when contact making.

To acknowledge the physical mechanism of adhesion force, the changes of contact force and joule heat during initial electrical contact are analyzed in more detail.

A. Physical Mechanism of Adhesion Force

As shown in Fig. 3, the adhesion phenomenon is obviously correlative with the current load case, so it is presumed that the adhesion force is related to the joule heat produced by the contact resistance during making. The softening point of Au is 100 °C (80 mV) and the melting point of Au is 1063 °C (430 mV).[25] Assuming that the highest asperity in contact needs to be plastically deformed, while the contact voltage value indicates that the contact temperature reaches the softening temperature, the plastic deformation of the asperities proceeds more rapidly and leads to an increase in the effective contact area. Therefore, the softening of the highest asperities on the contact surface leads to the noisy contact force behavior seen in the A-B stage compared with the no current load case. The nonlinear relationship between contact force and actuator position in Fig. 3 supports this claim. We define k the strain coefficient of the force sensor, δ the displacement of actuator, and $\delta^{'}$ the deformation caused by the softening and melting of the gold coating. Thus, the relationship between the contact force and time is expressed as

$$F_c = k[\delta - \delta\ '] = kv\left[t - t_0\left(1 - e^{-\frac{t}{\tau}}\right)\right] \text{ (1)}$$

where δ' is assumed a negative exponential function, $\delta' = \delta_0\left(1 - e^{-\frac{t}{\tau}}\right) = vt_0\left(1 - e^{-\frac{t}{\tau}}\right)$, and t_0 is the intersection between the linear part of the curve and the horizontal coordinate axis, which indirectly shows the delay time during softening process. Hence, δ_0 is the corresponding shift displacement and τ is the time constant in the softening process. As shown in Fig. 3, $k = 19.09$ mN/μm, $t_0 = 16.878$s, and $\tau = 21.754$ s and these numbers are the fitting results from Origin 9.0.

We also collected shift displacement δ_0 and time constant τ during each operation, and Fig. 5 shows the relationship between δ_0 and τ for 108 repetitive experimental results that are provided to ensure the accuracy of fitting. As shown in Fig. 5, the adjacent R-square of the fitting results is 0.7983, which means a significant linear correlation between δ_0 and τ.

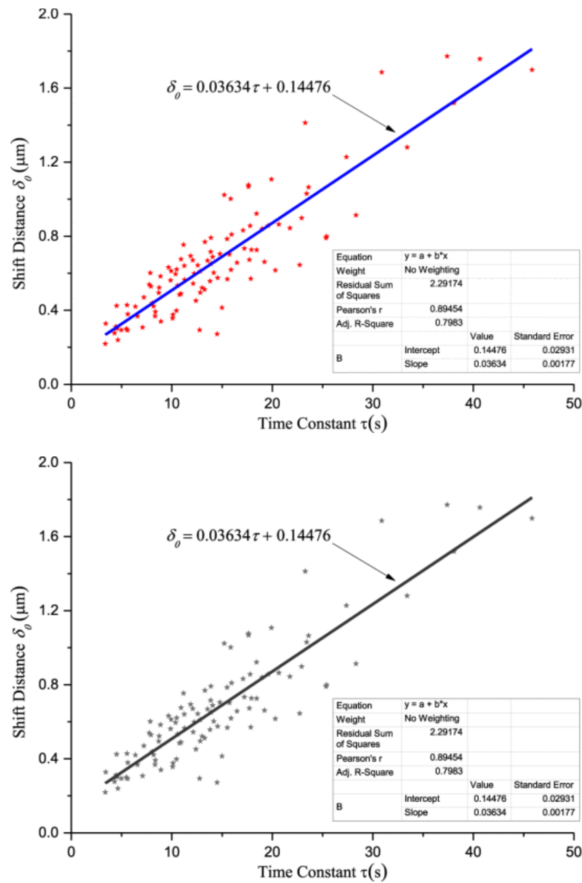

Fig. 5. Scatter diagram of δ_0 $-\tau$ under the conditions of 15 V/1 A and 50 nm/s.

The contact voltage of the A-B stage is less than 0.1 V, so the corresponding load current I can be taken as constant and the heat production power P_c of contact resistance is expressed as I^2R.. Heat is primarily dissipated by conduction and since the heat dissipation power P_s is also proportional to contact area, the heat accumulation power is given by

$$P = P_c - P_s = I^2R - 2\lambda A\frac{d\theta}{dl} \text{ (2)}$$

where λ is the heat conductivity, $(d\theta/dl)$ is the temperature gradient at contact interface, and A is the contact area. The dissipation rate of contact heat can be reflected by the time constant τ. When τ increases, the dissipation rate slows down and brings out the longer acting duration of contact heat, and at the same time, δ_0 goes up and thus there is a positive correlation relationship between δ_0 and τ.

In addition, time constant τ is closely correlated with the contact area A, which is equivalent to the dissipation area. Since the increase in the effective contact area results in the reduced contact resistance and the increased dissipated heat through conduction, which are followed by the shrink of heating power and the increment of cooling power. Hence, the duration for the contact temperature rise reaching stabilization is reduced.

The softening and melting of contact surface is partially dependent on the contact area A; when the contact temperature reaches the softening temperature, the plastic deformation of the asperities proceeds more rapidly and leads to an increase in the effective contact area,[26] and thus facilitates contact heat dissipation. Therefore, the lower τ implies that softening and melting produce substantial adhesion force. In the case of higher τ, under the same contact conditions, however, the measured weak adhesive force indicates that there are no obvious softening and melting asperities due to the slow thermal equilibrium process.

Fig. 6 shows the scatter diagram in terms of F_z and τ, which are the same results of Fig. 5. This suggests the above claim and analysis that the adhesive force is directly dependent on the time constant τ.

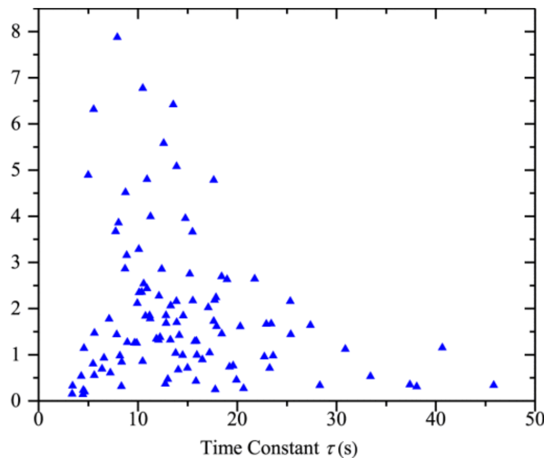

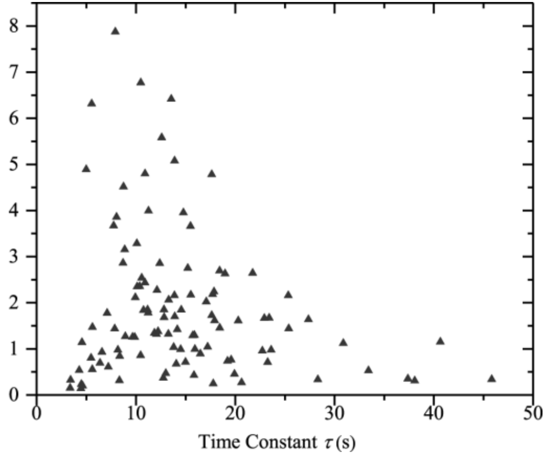

Fig. 6. Relationship between adhesion force F_z and time constant τ under the conditions of 15 V/1 A and 50 nm/s.

B. Relationship Between Adhesion Resistance and Adhesion Force

The moving and fixed electrodes are completely welding together in the D-E stage. As shown in Fig. 8, the adhesion force F_z is nearly inversely proportional to the contact resistance R_d. For a welding case, the tensile strength is defined as follows:

$$F_z = \sigma_b A_z \quad (3)$$

where σ_b is the tensile strength.[27] Therefore, the adhesion force F_z of gold-plated contacts is affected by the adhesion area A_z.

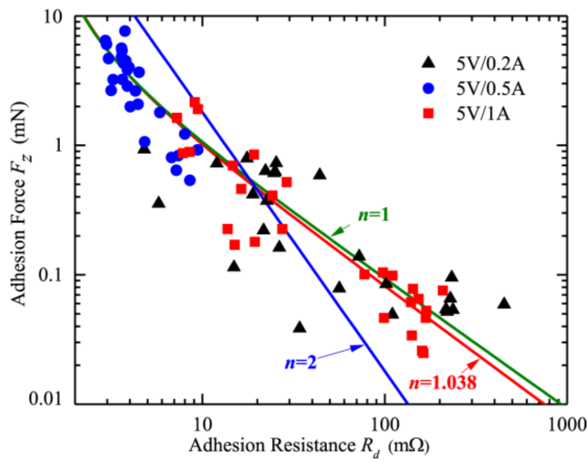

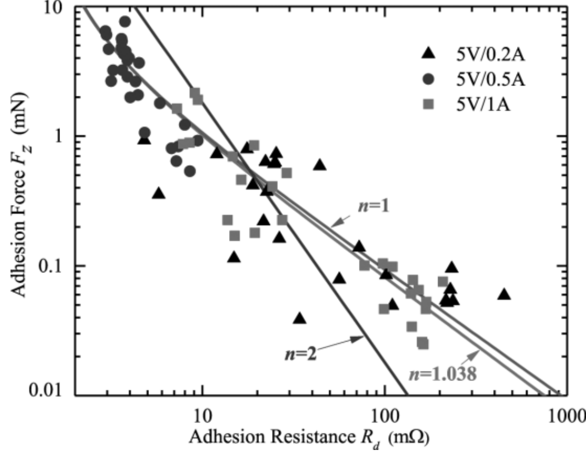

Fig. 8. Fitting results comparison with different indices n in double-logarithmic coordinate.

As known, the contact resistance R_d is made up of constriction resistance R_s and film resistance R_f.. Thus, based on the classical Holm's electrical contact theory,[26] R_d is given by

$$R_d = \frac{\sigma}{n\pi a_p^2} + \frac{\rho}{2na_p} \quad (4)$$

where ρ is the resistivity of the contact material, σ is the surface resistivity of the film, a_p is the radius of spots, and n is the number of spots. Assuming that there is no film resistance within the contact welding, it results in

$$R_d = \frac{\rho}{2}\left(\frac{A_p}{\pi}\right)^{-\frac{1}{2}} \quad (5)$$

where A_p is the total area of conductive spots, in which $A_p \approx A_z$. Combining (3) and (5), results in the following equation:

$$F_z = \frac{\pi\sigma_b\rho^2}{4} R_d^{-2} = C_1 R_d^{-2} \quad (6)$$

where $C_1 = \pi\sigma_b\rho^2/4$. For a typical bulk electrical junction, the current flow lines become increasingly distorted and bundle together to pass through the separate contact spots. Constriction of the current results in the reduction of effective conduction area and thus increases electrical resistance. The additional resistance is termed as constriction resistance.

The premise of (3) is important that the current-potential field in constriction region is completely symmetrical and the thickness of spot could be considered as zero or small enough (on the order of angstroms). The thickness of adhesion part is much larger than this order of magnitude when there is adhesion between contact interfaces. Hence, the physical model of contact resistance considering the thickness of adhesion parts is established, as shown in Fig. 7. In the adhesion case, total contact resistance is divided into constriction resistance $2R_{ss}$ and bulk resistance R_t, and thus the contact resistance could be given by

$$R_d = 2R_s + R_t = \frac{\rho}{2}\left(\frac{A_p}{\pi}\right)^{-\frac{1}{2}} + \rho l A_p^{-1} \quad (7)$$

in which l is the thickness of the adhesion part. When only the bulk resistance R_t is considered, the relationship between adhesion force F_z and contact resistance R_d is expressed by

$$F_z = \sigma_b A_z = \sigma_b \rho l R_d^{-1} = C_2 R_d^{-1} \quad (8)$$

where $C_2 = \rho l \sigma_b$. Using (6) and (8), the mathematical expression of adhesion force results in

$$F_z = C R_d^{-n} \quad (9)$$

where the range of the power exponent n is 1–2 and the coefficient C is related to the strain strength σ_b, resistivity ρ, and adhesion thickness l.

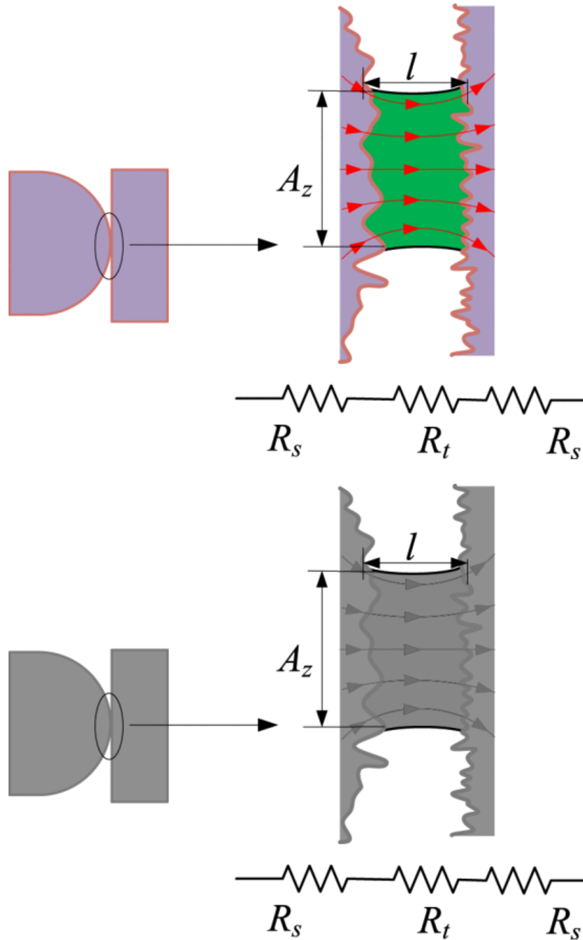

Fig. 7. Schematic of contact resistance during adhesion stage.

The actual measurement results of adhesion resistance always consist of the additional resistance R_0 in the circuit, which refers to the resistance of wire and clamping fixture connection part besides the contact resistance R_d. In another experiment, the measured additional resistance R_0 is about 1–2 mΩ (tin soldering the fixed and moving electrodes together). Therefore, this term could not be neglected during mathematical fitting and thus (9) is rewritten as

$$F_z = CR_d^{-n} = C(R_m - R_0)^{-n} \quad (10)$$

where R_m is the measured contact resistance. Fig. 8 shows the relationship between F_z and R_d with different current loads at a speed of 50 nm/s, an open voltage U of 5 V, and load currents I of 1, 0.5, and 0.2 A, respectively. As shown, when $R_d > 10\text{m}\Omega$, the adhesion force F_z is less than 1 mN. Meanwhile, when the contact resistance R_d is less than 10 mΩ, the adhesion force increases apparently and tends to be one of the asymptote (the additional resistance R_0)) with the decrease in resistance. When C, R_0, and n are free variables, the best fitting expression of the adhesion force in terms of the contact resistance obtained by Origin 9.0 is given by

$$F_z = 0.965(R_d - 1.278)^{-1.03}. \quad (11).$$

Fig. 8 also shows the fitting results comparison with different indices n in double-logarithmic coordinate. With the $F_z - R_d$ experimental data and (10) fitting, the index parameter n is selected as 1 and 2, and an independent variable. When n is designated as the independent variable, which is the best fitting power exponent of 1.03, the fitting result is $C = 0.965$ and $R\,0 = 1.278$. When $n = 1$, the fitting result is $C = 0.925$ and $R_0 = 1.303$, which is similar to the case of $n = 1.03$.

As shown in Table II, four different load voltages and motion speed condition combinations of 5 V/25 nm/s, 5 V/50 nm/s, 25 V/25 nm/s, and 25 V/50 nm/s are applied, and the fitted index parameter n is listed, respectively, in Table II. It is noted that the best fitting index n is from 0.92 to 1.27, which almost approaches to 1. Comparing with the case of $n = 1$, no substantial difference in fitting results is observed, but the results of $n = 2$ are much different from $n = n_0$. Therefore, it is reasonable to take $n = 1$ as the best fitting index for describing the relationship between adhesion force and contact resistance. From the above results, it is confirmed that the contact resistance is mainly bulk resistance of the welded nugget, and the constriction resistance adjacent to the interface is negligible. Hence, (8) can be used for expressing the relationship between F_z and R_d, then

$$C = C_2 = \rho l \sigma_b. \quad (12)$$

TABLE II Contrast of R-Square of Curves Under Different Conditions

Experimental conditions U(V)/v(nm/s)	Best fitting power n_0	Adj. R-square		
		n=1	n=n_0	n=2
5/25	1.03	0.811	0.813	-7.278
5/50	1.27	0.643	0.648	0.495
25/25	1.05	0.647	0.648	0.175
25/50	0.922	0.670	0.660	-0.309

Surface morphology of the gold-plated contacts after making/breaking is shown in Fig. 9. In this case, the measured adhesion force F_z is 2 mN, and the strain strength of gold is $\sigma_b = 140$ N/mm 2,[22] the resistivity is $\rho = 21.9\mu\Omega \cdot$ mm, and the contact resistance is calculated about 1.08 mΩ using (11). Furthermore, the thickness and area of the adhesion parts is estimated to 0.2 μm and 14 μm^2 using (3) and (12), respectively, and then the current density through the adhesion part is about 3.5×10^{10} A/ m^2 when the current is 0.5 A. As shown in Fig. 9, the stacked melting traces are almost circular in shape and the area of top one is 9.6 μm^2, which is consistent with the above estimation. And

the observed stacked melting traces are mainly attributed to the metal bridge characteristic, which is the fluctuation of intermittent contact bridge voltage after adhesion.

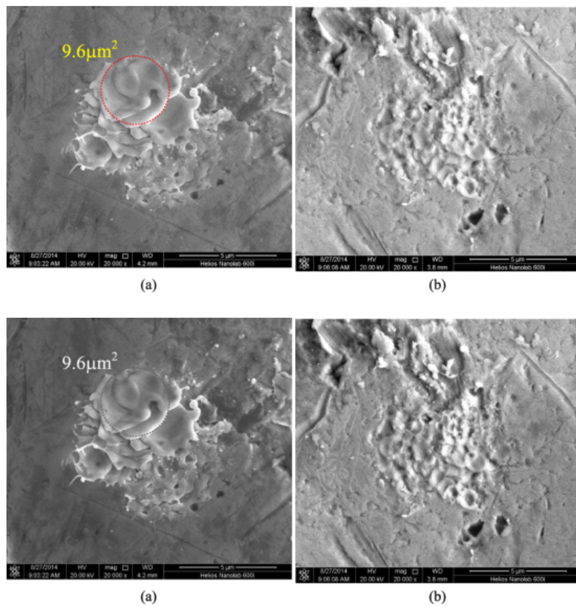

Fig. 9. Surface morphology of the gold-plated contacts after making/breaking (with a load voltage of 5 V, a load current of 0.5 A, and a speed of 25 nm/s). (a) Cathode. (b) Anode.

SECTION IV. Conclusion

We have measured the variations in contact voltage and contact force of Au-plated contacts as a function of piezoactuator position at a speed of 25 and 50 nm/s. The experimental results show that the slow velocity extends the joule heating duration, and the continuous joule heat lead to the partial highest asperities softening and melting during initial contact. That is the reason for the contact force curve being bending and the subsequent adhesion phenomena. The stronger adhesion force is attributed to the occurred higher initial contact temperature combined with the higher temperature decrease rate in making process. The correlation between adhesion force and adhesion resistance is confirmed as the inverse proportional function, which is a good indication that adhesion resistance is the bulk resistance of weld nugget. From these results, the adhesion behaviors of Au-to-Au contacts under current load conditions could be explained. In our opinion, the transient contact duration of making process needs to be reduced when designing and fabricating switches and metal contacts. It is expected that this preliminary study on the adhesion process and relative influencing factors will be useful for reducing the stiction failure probability of MEMS switches.

References

1. M. Braunovic, V. V. Konchits, N. K. Myshkin, Electrical Contacts Fundamentals Applications and Technology, New York, NY, USA:CRC Press, 2006.

2. Z.-K. Chen, G. J. Witter, "Electrical contacts for automotive applications: A review", *IEICE Trans. Electron.*, vol. E87-C, no. 8, pp. 1248-1254, 2004.

3. J. Swingler, J. W. McBride, C. Maul, "Degradation of road tested automotive connectors", *IEEE Trans. Compon. Packag. Technol.*, vol. 23, no. 1, pp. 157-164, Mar. 2000.

4. G. H. Gelinck, T. C. T. Geuns, D. M. de Leeuw, "High-performance all-polymer integrated circuits", *Appl. Phys. Lett.*, vol. 77, no. 10, pp. 1487-1489, 2000.

5. P. M. Hall, "Resistance calculations for thin film rectangles", *Thin Solid Films*, vol. 300, no. 1, pp. 256-264, 1997.

6. Y. Huang, A. S. S. Vasan, R. Doraiswami, M. Osterman, M. Pecht, "MEMS reliability review", *IEEE Trans. Device Mater. Rel.*, vol. 12, no. 2, pp. 482-493, Jun. 2012.

7. R. A. Coutu, J. R. Reid, R. Cortez, R. E. Strawser, P. E. Kladitis, "Microswitches with sputtered Au AuPd Au-on-AuPt and AuPtCu alloy electric contacts", *IEEE Trans. Compon. Packag. Technol.*, vol. 29, no. 2, pp. 341-349, Jun. 2006.

8. R. A. Coutu, P. E. Kladitis, K. D. Leedy, R. L. Crane, "Selecting metal alloy electric contact materials for MEMS switches", *J. Micromech. Microeng.*, vol. 14, no. 8, pp. 1157-1164, 2004.

9. M. Vincent et al., "Field emission and material transfer in microswitches electrical contacts", *Appl. Phys. Lett.*, vol. 97, no. 26, pp. 263503, 2010.

10. K. Komvopoulos, "Surface engineering and microtribology for microelectromechanical systems", *Wear*, vol. 200, no. 1, pp. 305-327, 1996.

11. Y.-P. Zhao, L. S. Wang, T. X. Yu, "Mechanics of adhesion in MEMS—A review", *J. Adhesion Sci. Technol.*, vol. 17, no. 4, pp. 519-546, 2003.

12. W. Ren, P. Wang, J. Song, G. Zhai, "Effects of current load on wear and fretting corrosion of gold-plated electrical contacts", *Tribol. Int.*, vol. 70, pp. 75-82, Feb. 2014.

13. S. Fouvry, P. Jedrzejczyk, P. Chalandon, "Introduction of an exponential formulation to quantify the electrical endurance of micro-contacts enduring fretting wear: Application to Sn Ag and Au coatings", *Wear*, vol. 271, no. 9, pp. 1524-1534, 2011.

14. V. Sabelkin, S. Mall, "Combined adhesion and friction effects on cylinder-on-flat elastic–plastic microcontact", *J. Adhesion Sci. Technol.*, vol. 23, no. 6, pp. 851-879, 2009.

15. R. P. Hennessy, N. E. McGruer, G. G. Adams, "Modeling of a thermal-electrical-mechanical coupled field contact", *J. Tribol.*, vol. 134, no. 4, pp. 041402, Sep. 2012.

16. X. Ye, H. Liang, J. Deng, G. Zhai, "Research on dynamic characteristics testing and analyzing system of electromagnetic relay", *IEICE Trans. Electron.*, vol. E92-C, no. 8, pp. 1028-1033, 2009.

17. H. Kwon et al., "Investigation of the electrical contact behaviors in Au-to-Au thin-film contacts for RF MEMS switches", *J. Micromech. Microeng.*, vol. 18, no. 10, pp. 105010, 2008.

18. J. W. Tringe, T. A. Uhlman, A. C. Oliver, J. E. Houston, "A single asperity study of Au/Au electrical contacts", *J. Appl. Phys.*, vol. 93, no. 8, pp. 4661, 2003.

19. S. T. Patton, J. S. Zabinski, "Fundamental studies of Au contacts in MEMS RF switches", *Tribol. Lett.*, vol. 18, no. 2, pp. 215-230, Feb. 2005.

20. G. Gregori, D. R. Clarke, "The interrelation between adhesion contact creep and roughness on the life of gold contacts in radio-frequency microswitches", *J. Appl. Phys.*, vol. 100, no. 9, pp. 094904, 2006.

21. K. Miyanaga, Y. Kayano, H. Inoue, "A study on separation of heat generation and heat transfer related to temperature rise of silver palladium contact", *IEICE Trans. Electron.*, vol. E89-C, no. 8, pp. 1129-1135, 2006.

22. K. Miyanaga, Y. Kayano, H. Inoue, "Effect of the thermal constant on temperature rise of silver palladium alloy contacts", *IEICE Trans. Electron.*, vol. E90-C, no. 7, pp. 1405-1411, 2007.

23. K. Miyanaga, Y. Kayano, T. Takagi, H. Inoue, "Effect of heating value on contact diameter at low speed breaking contact", *IEICE Trans. Electron.*, vol. E92-C, no. 8, pp. 1020-1022, 2009.

24. K. Miyanaga, Y. Kayano, T. Komakine, H. Inoue, "Effect of heat conductivity on bridge break at different material contact pairs", *IEICE Trans. Electron.*, vol. E94C, no. 9, pp. 1431-1434, 2011.

25. P. G. Slade, Electrical Contacts: Principles and Applications, New York, NY, USA:Marcel Dekker, 1999.

26. R. Holm, Electric Contacts: Theory and Application, New York, NY, USA:Springer-Verlag, 1967.

27. V. A. Keil, W. A. Merl, E. Vinaricky, Elektrische Kontakte und ihre Werkstoffe, New York, NY, USA:Springer-Verlag, 1984.